DOI: 10.1002/ejic.200600242

Methoxyphenyl-Functionalized Diiron Azadithiolates as Models for the Active Site of Fe-Only Hydrogenases: Synthesis, Structures, and Biomimetic H_2 Evolution

Li-Cheng Song,*[a] Jian-Hua Ge,[a] Xiao-Guang Zhang,[a] Yang Liu,[a] and Qing-Mei Hu[a]

Keywords: Biomimetic chemistry / Diiron azadithiolate / Iron-only hydrogenases / Structural elucidation / Catalytic H_2 evolution

A series of methoxyphenyl-functionalized diiron azadithiolate (ADT) complexes, [{(μ-SCH_2)$_2$N(C_6H_4OMe-*p*)}$Fe_2(CO)_5$L] [L = CO (**2**); PPh_3 (**3**); PPh_2H (**4**)] and [{(μ-SCH_2)$_2$N-(C_6H_4OMe-*p*)}$Fe_2(CO)_4(CN)_2$][Et_4N]$_2$ (**5**) as the active site models of Fe-only hydrogenases has been investigated. While model **2** was prepared in 67 % yield by a condensation reaction of *N*,*N*-bis(chloromethyl)-*p*-methoxyaniline (**1**) with [(μ-LiS)$_2Fe_2(CO)_6$], models **3**–**5** were prepared in 49–75 % yields by a CO substitution reaction of **2** with PPh_3, PPh_2H, or Et_4NCN, respectively. The X-ray crystal structures of **2** and **3** revealed that the methoxyphenyl substituent is attached to the N atom by an axial bond and the nitrogen lone electron pair in an equatorial position. On the basis of cyclic voltammetric studies of **2** and **4**, it was found that **2** is a catalyst for proton reduction, and an EECC mechanism is proposed for such electrocatalytic H_2 production catalyzed by the ADT-type models.

Introduction

Hydrogen evolution and uptake in the biological energy cycle is mostly catalyzed by two types of metalloenzymes: Fe-only hydrogenases and NiFe hydrogenases.[1,2] Fe-only hydrogenases (hereafter referred to as FeHases) have recently received much more attention than NiFe hydrogenases, primarily owing to their much higher efficiency than NiFe hydrogenases in the production of hydrogen,[3] a clean and highly efficient fuel. The high-quality crystal structures of FeHases isolated from *C. pasteurianum* and *D. desulfuricans* have indicated[4] that the active site of FeHases (so-called H cluster) comprises a butterfly 2Fe2S cluster with one of the Fe atoms linked to a cuboidal 4Fe4S cluster through the S atom of a cysteinyl ligand. There are also three other ligands, namely CO, CN^-, and dithiolate coordinated to Fe atoms of the butterfly 2Fe2S cluster (Scheme 1). It is noteworthy that the dithiolate ligand bridged between the two iron atoms of the 2Fe2S cluster was recently suggested as an azadithiolate (ADT) SCH_2NHCH_2S,[5] in which the bridgehead N atom plays an important role for the heterolytic cleavage or formation of H_2 in the enzymatic process.[6] In spite of the biological importance of the bridgehead N atom in the H cluster, the synthetic and functional studies regarding azadithiolate (ADT) model complexes[7] have been much less investigated than diiron 1,3-propanedithiolate (PDT) model compounds.[8] So far, the PDT-type models [(μ-H)(μ-PDT)$Fe_2(CO)_4(L)_2]^+$ (L = Me_3P, *t*BuNC) have been reported to be catalysts for H/D exchange reactions.[9] In addition, the PDT- and ADT-type models [(μ-PDT)$Fe_2(CO)_4(CN)(Me_3P)]^-$,[10] [(μ-PDT)Fe_2-$(CO)_4L_2$] (L = CO, Me_3P),[11] and [{(μ-SCH_2)$_2$N(*p*-$BrC_6H_4CH_2$)}$Fe_2(CO)_6$][12] have been demonstrated to be catalysts for proton reduction to H_2 under electrochemical conditions. To further develop the biomimetic chemistry of FeHases, we initiated a study on the synthesis, structures and properties of a new series of diiron ADT-type model complexes, in which some substituents are attached to the N atom and Fe atoms in the diiron ADT framework [{(μ-SCH_2)$_2$N}$Fe_2(CO)_n$] (*n* = 4, 5). Herein we report our results obtained from this study.

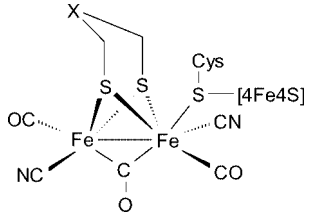

Scheme 1. Composite structure of H cluster obtained from protein crystallography (X = CH_2, NH, or O).

[a] Department of Chemistry, State Key Laboratory of Elemento-Organic Chemistry, Nankai University,
Tianjin 300071, China
Fax: +86-22-23504853
E-mail: lcsong@nankai.edu.cn

Results and Discussion

Synthesis and Spectroscopic Characterization of Compounds 1–5

The synthetic methods for our target compounds **2**–**5** and their precursor **1** are based on those previously reported by Rauchfuss[13] and the well-known CO substitution reactions with various 2e ligands[14] (Scheme 2). Treatment of *p*-methoxyaniline with paraformaldehyde in CH_2Cl_2 at room temperature followed by treatment with an excess of $SOCl_2$ gave *N*,*N*-bis(chloromethyl)-*p*-methoxyaniline (**1**) in 91% yield. Further reaction of **1** with lithium salt $[(\mu\text{-}LiS)_2Fe_2(CO)_6]$ {generated in situ from $[(\mu\text{-}S)_2Fe_2(CO)_6]$ and Et_3BHLi in THF at –78 °C}[15] afforded the ADT-type model **2** in 67% yield. Models **3**–**5** could be prepared in 49–75% yields through CO substitution reactions of **2** in MeCN with PPh_3 in the presence of the decarbonylating agent Me_3NO, with PPh_2H in toluene at reflux, or with Et_4NCN in MeCN from 0 °C to room temperature, respectively.

Compounds **1**–**5** have been characterized by elemental analysis and IR and ^1H NMR spectroscopy. The ^1H NMR spectra of **1**–**5** each show a singlet at $\delta \approx 3.7$ ppm for their MeO groups and an AB quartet between $\delta = 6.5$ and 7.2 ppm for their *para*-disubstituted C_6H_4 benzene rings. While precursor **1** displays a singlet at $\delta = 5.44$ ppm for its CH_2 groups, **2** exhibits a singlet, **3** two doublets, **4** a multiplet, and **5** a singlet for their CH_2 groups at a relatively higher field. In addition, the IR spectra of **2**–**5** show three absorption bands around 2000 cm^{-1} for their terminal carbonyl groups and the $\tilde{\nu}(C{\equiv}O)$ values of **3**–**5** are markedly shifted towards lower frequencies relative to those of their parent complex **2**. It follows that the PPh_3, PPh_2H, and CN^- ligands in **3**–**5** are all stronger electron-donating ligands than CO.[16]

Crystal Structures of Compounds 2 and 3

The structures of **2** and **3** have been unambiguously confirmed by X-ray crystal diffraction analysis. ORTEP diagrams of **2** and **3** are given in Figures 1 and 2, and Tables 1 and 2 list selected bond lengths and angles, respectively. Models **2** and **3**, as illustrated in Figures 1 and 2, indeed consist of a *p*-methoxyphenyl-substituted azadithiolate group that is bridged between two iron atoms to form a butterfly 2Fe2S cluster. The Fe–Fe bond of **3** [2.554(2) Å] is longer than those of **2** [2.5076(16) Å], $[\{(\mu\text{-}SCH_2)_2\text{-}NMe\}Fe_2(CO)_6]$ [2.4924(7) Å][7a] and $[(\mu\text{-}PDT)Fe_2(CO)_6]$ [2.5103(11) Å],[17] but somewhat shorter than those in the structures of enzymes *C. pasteurianum* and *D. desulfuricans* (ca. 2.6 Å).[4] The sum of the C–N–C angles around the N atom is 354.8° for **2** and 355.9° for **3**. This means that the p–π conjugation exists between the substituted benzene ring and the p-orbital of the bridgehead N atom, although it is weakened because the N atom is slightly deviated from the plane defined by the N(1), C(7), C(8), and C(9) atoms (for **2**) or by the N(1), C(24), C(25), and C(26) atoms (for **3**). Both **2** and **3** contain two fused six-membered rings: N(1)-C(7)S(1)Fe(2)S(2)C(8) and N(1)C(7)S(1)Fe(1)S(2)C(8) for **2**; N(1)C(24)S(1)Fe(1)S(2)C(25) and N(1)C(24)S(1)Fe(2)-S(2)C(25) for **3**. The former six-membered ring in **2** or **3** is in a chair conformation, while the latter ring in **2** or **3** is in a boat conformation. It should be noted that the phenyl group attached to the N(1) atom of **2** and **3** resides in an

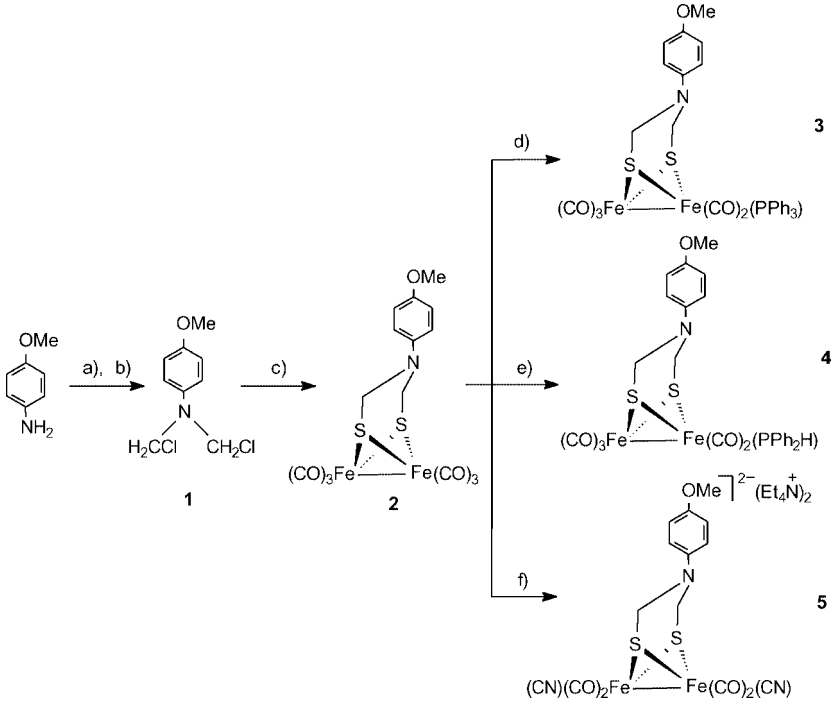

Scheme 2. (a) $(CH_2O)_n$, CH_2Cl_2, room temp.; (b) $SOCl_2$, room temp.; (c) $[(\mu\text{-}LiS)_2Fe_2(CO)_6]$, THF, –78 °C; (d) PPh_3, Me_3NO, MeCN, room temp.; (e) PPh_2H, toluene, reflux; (f) Et_4NCN, MeCN, 0 °C.

axial position and the nitrogen lone electron pair is in an equatorial position. In fact, such a conformation is also observed in other phenyl-substituted ADT-type models.[7c] Furthermore, the PPh_3 ligand in **3** is in an axial position of the square-pyramidal geometry of the Fe(1) atom and *trans* to the substituted benzene ring in order to reduce the steric repulsion between these two bulky structural units.

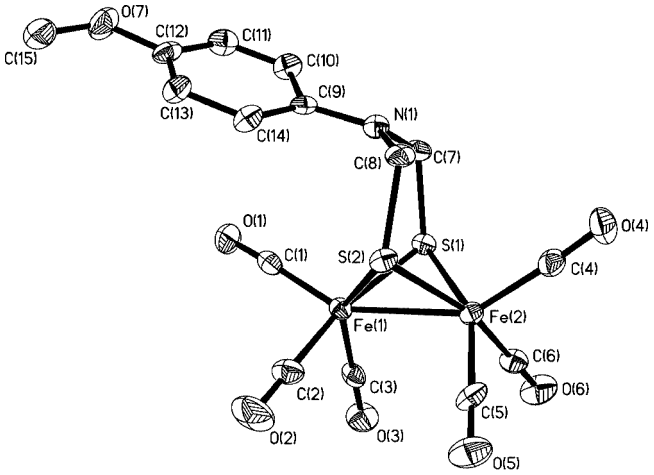

Figure 1. ORTEP view of **2** with 30% probability level ellipsoids.

Table 1. Selected bond lengths [Å] and angles [°] for **2**.

Fe(1)–S(2)	2.264(3)	N(1)–C(7)	1.439(8)
Fe(2)–S(1)	2.263(2)	N(1)–C(8)	1.418(8)
Fe(1)–S(1)	2.2537(19)	N(1)–C(9)	1.419(8)
Fe(1)–Fe(2)	2.5076(16)	Fe(2)–S(2)	2.249(3)
S(1)–Fe(1)–S(2)	84.42(8)	Fe(1)–S(1)–Fe(2)	67.45(6)
S(1)–Fe(1)–Fe(2)	56.45(5)	Fe(2)–S(2)–Fe(1)	67.50(8)
S(2)–Fe(1)–Fe(2)	55.97(7)	C(8)–N(1)–C(9)	119.6(5)
S(2)–Fe(2)–Fe(1)	56.54(8)	C(8)–N(1)–C(7)	113.4(6)
S(1)–Fe(2)–Fe(1)	56.10(5)	C(9)–N(1)–C(7)	121.8(5)

Table 2. Selected bond lengths [Å] and angles [°] for **3**.

Fe(1)–P(1)	2.290(2)	Fe(2)–S(1)	2.322(2)
Fe(1)–S(1)	2.314(3)	P(1)–C(6)	1.856(7)
Fe(1)–S(2)	2.320(3)	N(1)–C(24)	1.443(8)
Fe(1)–Fe(2)	2.554(2)	N(1)–C(25)	1.452(9)
Fe(2)–S(2)	2.296(3)	N(1)–C(26)	1.438(9)
S(1)–Fe(1)–P(1)	105.13(8)	S(2)–Fe(2)–S(1)	83.44(8)
S(1)–Fe(1)–S(2)	83.09(8)	S(1)–Fe(2)–Fe(1)	56.43(7)
P(1)–Fe(1)–Fe(2)	156.84(7)	Fe(1)–S(1)–Fe(2)	66.84(8)
S(1)–Fe(1)–Fe(2)	56.73(6)	C(26)–N(1)–C(24)	118.6(6)
S(2)–Fe(1)–Fe(2)	55.96(7)	C(25)–N(1)–C(24)	114.2(6)

Electrochemistry of Compounds 2 and 4

The electrochemical behavior of the representative models **2** and **4** was studied in MeCN by cyclic voltammetric techniques. Table 3 lists their electrochemical data, and Figures 3 and 4 show their cyclic voltammograms, respectively.

Table 3. Electrochemical data of **2** and **4**.[a]

Compound	E_{pc}	E_{pa} [V]	E_{pa}	E_{pc} [V]
2	–1.61	–1.48	+0.48	–
	–2.10	–	+0.81	–
4	–1.78	–1.50	+0.26	–
	–2.22	–	+0.49	–

[a] All potentials in Table 3 are vs. Fc/Fc^+.

It has been demonstrated that **2** displays one quasi-reversible reduction, one irreversible reduction and two irreversible oxidations, whereas **4** exhibits two irreversible reductions and two irreversible oxidations. The first and second reduction peaks of **2** (–1.61 V, –2.10 V) and **4** (–1.78 V, –2.22 V) can be assigned to the one-electron reduction processes from Fe^IFe^I to Fe^IFe^0 and Fe^IFe^0 to Fe^0Fe^0 (supported by bulk electrolysis). Similarly, the first and second oxidation peaks of **2** (+0.48 V, +0.81 V) and **4** (+0.26 V, +0.49 V) should be attributed to the one-electron oxidation processes from Fe^IFe^I to Fe^IFe^{II} and Fe^IFe^{II} to

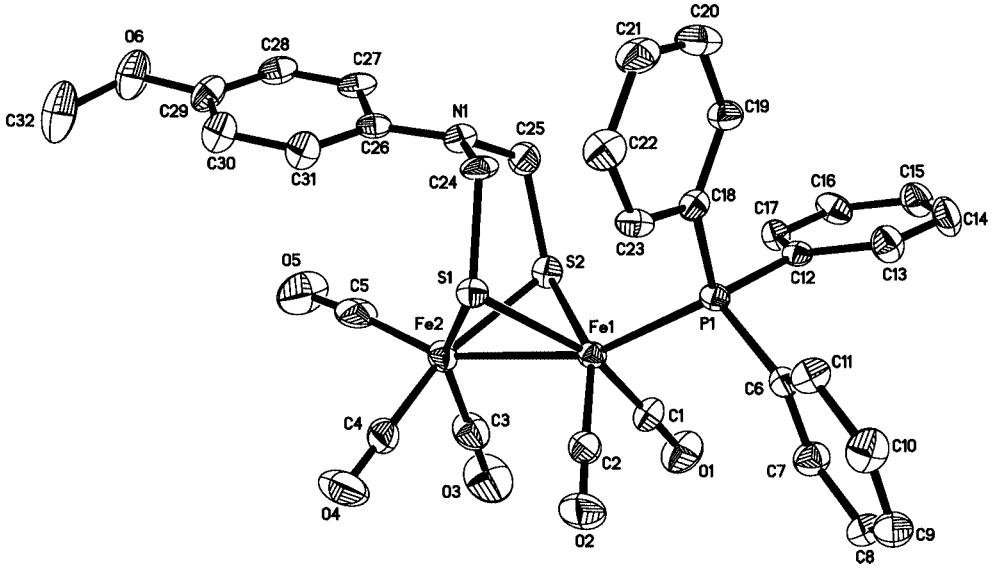

Figure 2. ORTEP view of **3** with 30% probability level ellipsoids.

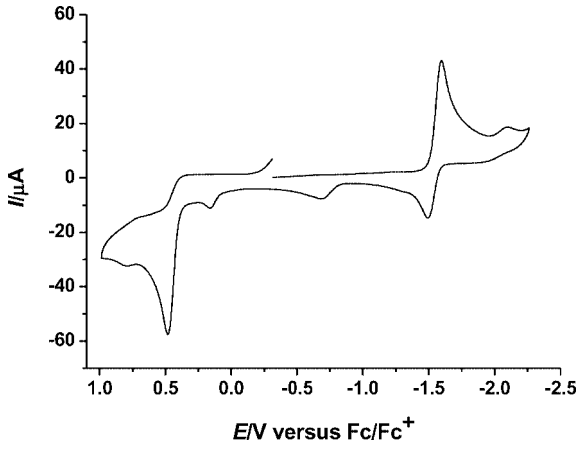

Figure 3. Cyclic voltammogram of **2** (1 mM) in 0.1 M nBu_4NPF_6/MeCN at a scan rate of 100 mVs^{-1}.

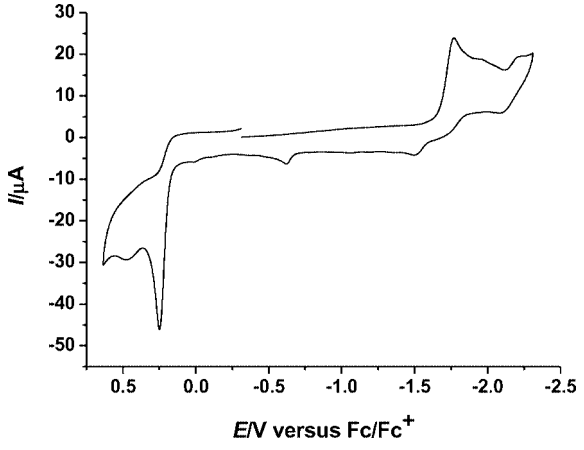

Figure 4. Cyclic voltammogram of **4** (1 mM) in 0.1 M nBu_4NPF_6/MeCN at a scan rate of 100 mVs^{-1}.

$Fe^{II}Fe^{II}$, respectively. It can be seen that the reduction and oxidation peaks of **4** (Figure 4) are apparently shifted towards more negative potentials than those corresponding to **2**. This is consistent with the substituent PPh_2H being a stronger electron-donating ligand than CO. Actually, the electrochemical behavior described above resembles that displayed by those reported for ADT-, PDT-, and ODT-(oxadithiolate)-bridged analogs.[10–12,18]

We further studied the electrochemical behavior of model **2** by cyclic voltammetric techniques in the presence of HOAc (0–10 mM) in MeCN. As shown in Figure 5, the current intensity of the initial first peak at –1.61 V slightly increased when the first amount of HOAc (2 mM) was added, but it did not increase further with sequential increments of the acid concentration. However, when the first 2 mM HOAc was added, the initial second peak at –2.10 V grew considerably and increased linearly with increasing acid concentration. It is evident that such cyclic voltammetric behavior features an electrocatalytic proton reduction process.[10–12,18–21] This catalytic process was further confirmed by electrolysis of a MeCN solution of **2** (0.33 mM) with excess HOAc (6.6 mM) at –2.18 V (Figure 6). The initial rate of electrolysis is more than twice as much as it is in the absence of the catalyst. A total of 10.2 F/mol passed in 0.5 h, which corresponds to 5.1 turnovers. In such a large-scale experiment, H_2 evolution could clearly be seen. Gas chromatographic analysis showed that the hydrogen yield was about 90%.

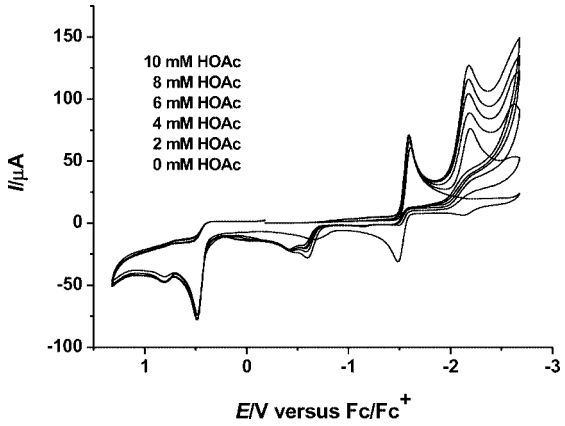

Figure 5. Cyclic voltammogram of **2** (1.0 mM) with HOAc (0–10 mM).

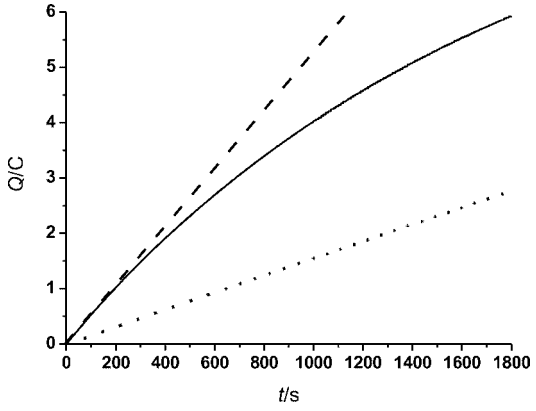

Figure 6. Bulk electrolysis of HOAc at a vitreous carbon rod electrode in the presence of **2** (——) and without **2** (·····); extrapolation of the catalytic reduction at the initial electrolysis rate (------).

On the basis of previously reported, similar cases[10–12,18–21] and the above-mentioned electrochemical observations, we can propose an EECC (E = electrochemical, C = chemical) mechanism to account for the above-described electrocatalytic H_2 production process. As shown in Scheme 3, model **2** can undergo a one-electron reduction at –1.61 V to give the intermediate **2a**. Further one-electron reduction of **2a** at –2.10 V affords intermediate **2b**, which is then protonated to give intermediate **2c**. Final protonation of **2c** results in H_2 evolution to accomplish the catalytic cycle. Apparently, this mechanism is different from the CECE mechanism for H_2 production from $HClO_4$ catalyzed by the benzyl-substituted model $[\{(\mu\text{-}SCH_2)_2N(p\text{-}BrC_6H_4CH_2)\}Fe_2(CO)_6]$.[12] In the CECE mechanism the bridged N atom of the benzyl-substituted model is first protonated by strong acid, $HClO_4$, whereas in our EECC mechanism the bridged N atom of model **2** is not protonated by weak acid, HOAc. In fact, the protonation of the benzyl-substituted model and the nonprotonation of **2** were

all confirmed by spectroscopic studies. That is, the ^1H NMR and IR spectroscopic data of the benzyl-substituted model determined in $HClO_4$ were obviously changed due to protonation of its bridged N atom,[12] while the corresponding data of model **2** determined by us in HOAc were almost the same as those determined in the absence of HOAc.[22] Finally, it should be noted that model **2** undergoes serious decomposition in $HClO_4$. The decomposition could be observed by its color changes from red to orange and then to light yellow. In addition, some bubbles were liberated upon addition of 5–30 equiv. of $HClO_4$ to a solution of **2** in CD_3CN. In fact, it is the decomposition that precluded us from further studies on its electrochemical behavior in the presence of $HClO_4$.

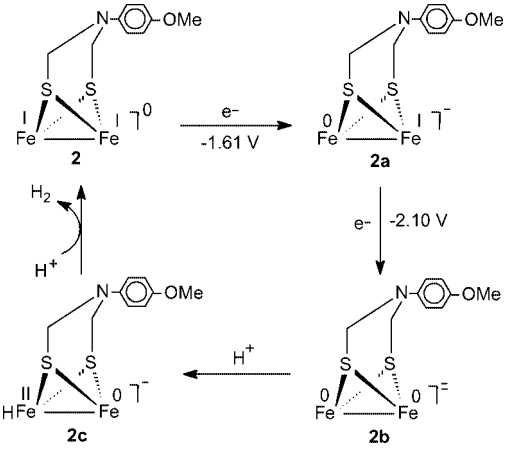

Scheme 3. Suggested EECC mechanism for H_2 production catalyzed by **2**. All carbonyl groups attached to Fe are omitted for clarity.

Experimental Section

General Comments: All reactions were carried out under prepurified nitrogen with standard Schlenk and vacuum-line techniques. All solvents were dried and distilled prior to use. Paraformaldehyde, $SOCl_2$, Et_3BHLi (1 M in THF), *p*-$MeOC_6H_4NH_2$, Et_4NCN, $Me_3NO{\cdot}2H_2O$, and PPh_3 were available commercially and used as received. $[(\mu\text{-}S)_2Fe_2(CO)_6]$[15] and PPh_2H[23] were prepared according to published procedures. Preparative TLC was carried out on glass plates (26 × 20 × 0.25 cm) coated with silica gel H (10–40 μm). IR spectra were recorded with a Nicolet Magna 560 FTIR or a Bruker Vector 22 infrared spectrophotometer. ^1H NMR spectra were recorded with a Bruker AC-P 300 NMR spectrometer. Elemental analyses was performed with an Elementar Vario EL analyzer. Melting points were determined with a Yanaco MP-500 apparatus.

Preparation of *N*,*N*-$(ClCH_2)_2N(C_6H_4OMe\text{-}p)$ (1): A suspension consisting of paraformaldehyde (1.50 g, 50 mmol), *p*-$MeOC_6H_4NH_2$ (2.46 g, 20 mmol), and CH_2Cl_2 (30 mL) was stirred at room temperature for 5 h, and then treated dropwise with $SOCl_2$ (9.52 g, 80 mmol). After the gas evolution had ceased, solvent and unreacted $SOCl_2$ were removed in vacuo. The residue was purified by extraction into Et_2O. Removal of Et_2O afforded **1** as an orange solid (3.99 g, 91%). M.p. 38–40 °C. ^1H NMR (300 MHz, $CDCl_3$): δ = 7.15, 7.12, 6.84, 6.81 (AB q, 4 H, C_6H_4), 5.44 (s, 4 H, $2CH_2$), 3.70 (s, 3 H, CH_3) ppm. IR (KBr disk): $\tilde{\nu}$ = 1507 (s), 1280 (m), 1245 (s), 1183 (m), 1154 (s), 1098 (m), 1052 (m), 1023 (s), 943 (s), 820 (s) cm^{-1}. $C_9H_{11}Cl_2NO$ (220.10): calcd. C 49.11, H 5.04, N 6.36; found C 49.12, H 5.19, N 6.40.

Preparation of $[\{(\mu\text{-}SCH_2)_2N(C_6H_4OMe\text{-}p)\}Fe_2(CO)_6]$ (2): A solution of $[(\mu\text{-}S)_2Fe_2(CO)_6]$ (0.344 g, 1 mmol) in THF (20 mL) was cooled to –78 °C and treated dropwise with Et_3BHLi (1 M in THF, 2 mL, 2 mmol) to give a green solution. After stirring for 15 min, **1** (0.55 g, 2.50 mmol) was added to cause an immediate color change from green to red. The mixture was warmed to room temperature and stirred for 8 h. The crude product was separated by TLC using CH_2Cl_2/petroleum ether (1:5) as the eluent. Compound **2** was obtained from the main band as a red solid (0.329 g, 67%). M.p. 132–135 °C. ^1H NMR (300 MHz, $CDCl_3$): δ = 6.90, 6.87, 6.72, 6.69 (AB q, 4 H, C_6H_4), 4.26 (s, 4 H, 2 CH_2), 3.78 (s, 3 H, CH_3) ppm. IR (KBr disk): $\tilde{\nu}$ = 2073 (s), 2027 (vs), 1969 (s) (C≡O) cm^{-1}. $C_{15}H_{11}Fe_2NO_7S_2$ (493.07): calcd. C 36.54, H 2.25, N 2.84; found C 36.42, H 2.30, N 2.86.

Preparation of $[\{(\mu\text{-}SCH_2)_2N(C_6H_4OMe\text{-}p)\}Fe_2(CO)_5(PPh_3)]$ (3): A mixture of **2** (0.124 g, 0.25 mmol), PPh_3 (0.065 g, 0.25 mmol), $Me_3NO{\cdot}2H_2O$ (0.029 g, 0.25 mmol), and MeCN (20 mL) was stirred at room temperature for 3 h. The resulting dark-brown mixture was concentrated to dryness in vacuo and the residue was separated by TLC using CH_2Cl_2/petroleum ether (1:2) as the eluent. Compound **3** was obtained from the main band as a red solid (0.136 g, 75%). M.p. 134 °C (dec). ^1H NMR (300 MHz, $CDCl_3$): δ = 7.73–7.44 (m, 15 H, $3C_6H_5$), 6.76, 6.73, 6.49, 6.46 (AB q, 4 H, C_6H_4), 3.82 (d, J = 12.3 Hz, 2 H, 2 C*H*H), 3.73 (s, 3 H, CH_3), 2.90 (d, J = 12.3 Hz, 2 H, 2 C*H*H) ppm. IR (KBr disk): $\tilde{\nu}$ = 2041 (vs), 1984 (vs), 1923 (s) (C≡O) cm^{-1}. $C_{32}H_{26}Fe_2NO_6PS_2$ (727.33): calcd. C 52.84, H 3.60, N 1.93; found C 52.80, H 3.45, N 1.87.

Preparation of $[\{(\mu\text{-}SCH_2)_2N(C_6H_4OMe\text{-}p)\}Fe_2(CO)_5(PPh_2H)]$ (4): A mixture of **2** (0.124 g, 0.25 mmol), PPh_2H (0.047 g, 0.25 mmol), and toluene (20 mL) was stirred and refluxed for 4.5 h. The same workup used for **3** gave **4** as a red solid (0.080 g, 49%). M.p. 126–127 °C. ^1H NMR (300 MHz, $CDCl_3$): δ = 7.62–7.34 (m, 10 H, 2 C_6H_5), 6.72, 6.69, 6.51, 6.48 (AB q, 4 H, C_6H_4), 6.20 (d, J = 349.8 Hz, 1 H, PH), 4.03–3.92 (m, 4 H, $2CH_2$), 3.68 (s, 3 H, CH_3) ppm. IR (KBr disk): $\tilde{\nu}$ = 2045 (vs), 1984 (vs), 1924 (s) (C≡O) cm^{-1}. $C_{26}H_{22}Fe_2NO_6PS_2$ (651.25): calcd. C 47.95, H 3.40, N 2.15; found C 47.92, H 3.32, N 2.19.

Preparation of $[\{(\mu\text{-}SCH_2)_2N(C_6H_4OMe\text{-}p)\}Fe_2(CO)_4(CN)_2]\text{-}[(Et_4N)]_2$ (5): A solution of Et_4NCN (0.156 g, 1 mmol) in MeCN (5 mL) was added to a solution of **2** (0.247 g, 0.5 mmol) in MeCN (20 mL) at 0 °C, causing an immediate gas evolution. The mixture was warmed to room temperature and stirred for 4 h. The resulting brown-red solution was concentrated to dryness and the product was washed with hexane and diethyl ether, and finally dried in vacuo. Compound **5** was obtained as a red solid (0.266 g, 71%). M.p. 82–83 °C. ^1H NMR (300 MHz, CD_3CN): δ = 6.86, 6.83, 6.72, 6.68 (AB q, 4 H, C_6H_4), 4.16 (s, 3 H, OCH_3), 3.74 (s, 4 H, 2 CH_2S), 3.44 (q, J = 6.9 Hz, 16 H, 8 CH_2CH$_3$), 1.14 (t, J = 6.9 Hz, 24 H, 8 CH_2CH_3) ppm. IR (KBr disk): $\tilde{\nu}$ = 2066 (s), 2027 (s) (C≡N), 1968 (vs), 1933 (vs), 1893 (vs) (C≡O) cm^{-1}. $C_{31}H_{51}Fe_2N_5O_5S_2$ (749.59): C 49.67, H 6.86, N 9.34; found C 49.50, H 7.02, N 9.21.

X-ray Structure Determination of 2 and 3: Single crystals of **2** and **3** suitable for X-ray diffraction analyses were grown by slow concentration of their CH_2Cl_2/haxane solutions at about –25 °C. Each single crystal was mounted on a Bruker SMART 1000 automated diffractometer. Data were collected at room temperature, using graphite-monochromated Mo-K_α radiation (λ = 0.71073 Å) in the ω-2θ scanning mode. Absorption corrections were performed with the SADABS program.[24] The structures were solved by direct

methods using the SHELXS-97[25] program and refined by full-matrix least-squares techniques (SHELXL-97[26]) on F^2. Hydrogen atoms were located by using the geometric method. Details of crystal data, data collections, and structure refinements are summarized in Table 4. CCDC-293719 (**2**) and -293720 (**3**) contain the supplementary crystallographic data for this paper. These data can be obtained free of charge from The Cambridge Crystallographic Data Centre via www.ccdc.cam.ac.uk/data_request/cif.

Table 4. Crystal data and structural refinement details for **2** and **3**.

	2	**3**
Empirical formula	$C_{15}H_{11}Fe_2NO_7S_2$	$C_{32}H_{26}Fe_2NO_6PS_2$
M_r [g·mol^{-1}]	493.07	727.33
Crystal system	orthorhombic	triclinic
Space group	*Pca*2(1)	$P\bar{1}$
a [Å]	15.995(4)	9.691(8)
b [Å]	9.306(3)	10.371(8)
c [Å]	24.928(8)	17.578(16)
α [°]	90	72.857(12)
β [°]	90	78.003(18)
γ [°]	90	87.556(13)
V [Å^3]	3710.7(19)	1651(2)
Z	8	2
$\rho_{calcd.}$ [g·cm^{-3}]	1.765	1.463
F(000)	1984	744
μ [mm^{-1}]	1.826	1.097
$2\theta_{max}$ [°]	52.98	50.02
Reflections collected	20521	8267
Independent reflections	6006	5706
Index ranges	$-20 \le h \le 1\,9$	$-11 \le h \le 9$
	$-11 \le k \le 9$	$-12 \le k \le 12$
	$-22 \le l \le 31$	$-16 \le l \le 20$
R	0.0463	0.0806
Rw	0.0921	0.1324
Goodness-of-fit	1.058	1.019
Largest diff peak/hole [e·Å^{-3}]	1.136/–0.448	0.731/–0.519

Electrochemistry: Acetonitrile (Fisher Chemicals, HPLC grade) was the solvent used for the electrochemistry. A solution of 0.1 M nBu$_4$NPF$_6$ in MeCN was used as the electrolyte in all of the cyclic voltammetric experiments. The electrolyte solution was degassed by bubbling N_2 through it for 10 min before measurements were taken. Electrochemical measurements were made using a BAS Epsilon potentiostat. All voltammograms were obtained in a three-electrode cell with a 3-mm-diameter glassy carbon working electrode, a platinum counter electrode and an Ag/Ag$^+$ (0.01 M AgNO$_3$/0.1 M nBu$_4$NPF$_6$ in MeCN) reference electrode under N_2 or CO. The working electrode was polished with 0.05 μm alumina paste and sonicated in water for 10 min. Bulk electrolysis was run on a vitreous carbon rod (ca. 3 cm^2) in a two-compartment, gas tight, H-type electrolysis cell containing ca. 18 mL of MeCN. All potentials are quoted against the ferrocene/ferrocenium (Fc/Fc$^+$) potential.

Acknowledgments

We are grateful to the National Natural Science Foundation of China and the Specialized Research Fund for the Doctoral Program of Higher Education of China for financial support of this work.

[1] a) M. Y. Darensbourg, E. J. Lyon, J. J. Smee, *Coord. Chem. Rev.* **2000**, *206–207*, 533–561; b) M. Y. Darensbourg, E. J. Lyon, X. Zhao, I. P. Georgakaki, *Proc. Natl. Acad. Sci. U. S. A.* **2003**, *100*, 3683–3688; c) D. J. Evans, C. J. Pickett, *Chem. Soc. Rev.* **2003**, *32*, 268–275; d) X. Liu, S. K. Ibrahim, C. Tard, C. J. Pickett, *Coord. Chem. Rev.* **2005**, *249*, 1641–1652.

[2] a) M. Frey, *ChemBioChem* **2002**, *3*, 153–160; b) S. P. J. Albracht, *Biochem. Acta* **1994**, *1188*, 167–204; c) A. Volbeda, M. H. Charon, C. Piras, E. C. Hatchikian, M. Frey, J. C. Fontecilla-Camps, *Nature* **1995**, *373*, 580–587; d) R. Cammack, *Nature* **1999**, *397*, 214–215; e) M. W. W. Adams, E. I. Stiefel, *Science* **1998**, *282*, 1842–1843; f) J. Alper, *Science* **2003**, *299*, 1686–1687.

[3] M. W. W. Adams, *Biochim. Biophys. Acta* **1990**, *1020*, 115–145.

[4] a) J. W. Peters, W. N. Lanzilotta, B. J. Lemon, L. C. Seefeldt, *Science* **1998**, *282*, 1853–1858; b) Y. Nicolet, C. Piras, P. Legrand, C. E. Hatchikian, J. C. Fontecilla-Camps, *Struct. (London)* **1999**, *7*, 13–23.

[5] a) Y. Nicolet, B. J. Lemon, J. C. Fontecilla-Caps, J. W. Peters, *Trends Biochem. Sci.* **2000**, *25*, 138–143; b) Y. Nicolet, A. L. Lacey, X. Vernede, V. M. Fernandez, E. C. Hatchikian, J. C. Fontecilla-Camps, *J. Am. Chem. Soc.* **2001**, *123*, 1596–1601.

[6] H. Fan, M. B. Hall, *J. Am. Chem. Soc.* **2001**, *123*, 3828–3829.

[7] a) J. D. Lawrence, H. Li, T. B. Rauchfuss, M. Bénard, M.-M. Rohmer, *Angew. Chem. Int. Ed.* **2001**, *40*, 1768–1771; b) H. Li, T. B. Rauchfuss, *J. Am. Chem. Soc.* **2002**, *124*, 726–727; c) S. Ott, M. Kritikos, B. Åkermark, L. Sun, *Angew. Chem. Int. Ed.* **2003**, *42*, 3285–3288.

[8] a) X. Zhao, I. P. Georgakaki, M. L. Miller, J. C. Yarbrough, M. Y. Darensbourg, *J. Am. Chem. Soc.* **2001**, *123*, 9710–9711; b) F. Gloaguen, J. D. Lawrence, M. Schmidt, S. R. Wilson, T. B. Rauchfuss, *J. Am. Chem. Soc.* **2001**, *123*, 12518–12527; c) E. J. Lyon, I. P. Georgakaki, J. H. Reibenspies, M. Y. Darensbourg, *J. Am. Chem. Soc.* **2001**, *123*, 3268–3278; d) M. Razavet, S. C. Davies, D. L. Hughes, J. E. Barclay, D. J. Evans, S. A. Fairhurst, X. Liu, C. J. Pickett, *Dalton Trans.* **2003**, 586–595.

[9] a) X. Zhao, I. P. Georgakaki, M. L. Miller, R. Mejia-Rodriguez, C.-Y. Chiang, M. Y. Darensbourg, *Inorg. Chem.* **2002**, *41*, 3917–3928; b) J. L. Nehring, D. M. Heinekey, *Inorg. Chem.* **2003**, *42*, 4288–4292.

[10] F. Gloaguen, J. D. Lawrence, T. B. Rauchfuss, *J. Am. Chem. Soc.* **2001**, *123*, 9476–9477.

[11] D. Chong, I. P. Georgakaki, R. Mejia-Rodriguez, J. Sanabria-Chinchilla, M. P. Soriaga, M. Y. Darensbourg, *Dalton Trans.* **2003**, 4158–4163.

[12] S. Ott, M. Kritikos, B. Åkermark, L. Sun, R. Lomoth, *Angew. Chem. Int. Ed.* **2004**, *43*, 1006–1009.

[13] J. D. Lawrence, H. Li, T. B. Rauchfuss, *Chem. Commun.* **2001**, 1482–1483.

[14] L.-C. Song, *Acc. Chem. Res.* **2005**, *38*, 21–28.

[15] D. Seyferth, R. S. Henderson, L.-C. Song, *Organometallics* **1982**, *1*, 125–133.

[16] J. P. Collman, L. S. Hegedus, J. R. Norton, R. G. Finke, *Principles and Applications of Organotransition Metal Chemistry*, 2nd ed., University Science Books, Mill Valley, CA, **1987**.

[17] E. J. Lyon, I. P. Georgakaki, J. H. Reibenspies, M. Y. Darensbourg, *Angew. Chem. Int. Ed.* **1999**, *38*, 3178–3180.

[18] L.-C. Song, Z.-Y. Yang, H.-Z. Bian, Y. Liu, H.-T. Wang, X.-F. Liu, Q.-M. Hu, *Organometallics* **2005**, *24*, 6126–6135.

[19] I. Bhugun, D. Lexa, J.-M. Saveant, *J. Am. Chem. Soc.* **1996**, *118*, 3982–3983.

[20] T. Liu, M. Wang, Z. Shi, H. Cui, W. Dong, J. Chen, B. Åkermark, L. Sun, *Chem. Eur. J.* **2004**, *10*, 4474–4479.

[21] R. Mejia-Rodriguez, D. Chong, J. H. Reibenspies, M. P. Soriaga, M. Y. Darensbourg, *J. Am. Chem. Soc.* **2004**, *126*, 12004–12014.

[22] The ^{1}H NMR (CD$_3$CN) data of **2** in HOAc are: δ = 7.02, 6.99, 6.91, 6.89 (AB q, 4 H, C$_6$H$_4$), 4.49 (s, 4 H, 2 CH$_2$), 3.85 (s, 3 H, CH$_3$) ppm. The IR (CH$_3$CN) data are: $\tilde{\nu}$ = 2074 (s), 2037 (vs), 1995 (vs) (C≡O) cm^{-1}. The ^{1}H NMR (CD$_3$CN) data of **2** without HOAc are: δ = 7.02, 6.99, 6.91, 6.89 (AB q, 4 H, C$_6$H$_4$), 4.49 (s, 4 H, 2 CH$_2$), 3.85 (s, 3 H, CH$_3$) ppm. The IR

(CH_3CN) data are $\tilde{\nu}$ = 2072 (s), 2037 (vs), 1995 (vs) (C≡O) cm^{-1}.
[23] W. Kuchen, H. Buchwald, *Chem. Ber.* **1958**, *91*, 2871–2877.
[24] G. M. Sheldrick, *SADABS, A Program for Empirical Absorption Correction of Area Detector Data*, University of Göttingen, Germany, **1996**.
[25] G. M. Sheldrick, *SHELXS97, A Program for Crystal Structure Solution*, University of Göttingen, Germany, **1997**.
[26] G. M. Sheldrick, *SHELXL97, A Program for Crystal Structure Refinement*, University of Göttingen, Germany, **1997**.
Received: March 19, 2006
Published Online: July 3, 2006

